Structure of a Serine Protease Proteinase K from *Tritirachium album limber* at 0.98 Å Resolution[†]

Christian Betzel,[‡] S. Gourinath,[§] Pravindra Kumar,[§] Punit Kaur,[§] Markus Perbandt,[‡] Susanne Eschenburg,[‡] and Tej P. Singh*[,§]

Institute of Medical Biochemistry and Molecular Biology, UKE, c/o DESY, Building 22a, Notkestrasse 85, 22603 Hamburg, Germany, and Department of Biophysics, All India Institute of Medical Sciences, New Delhi 110 029, India

Received November 3, 2000; Revised Manuscript Received January 8, 2001

ABSTRACT: X-ray diffraction data at atomic resolution to 0.98 Å with 136 380 observed unique reflections were collected using a high quality proteinase K crystals grown under microgravity conditions and cryocooled. The structure has been refined anisotropically with REFMAC and SHELX-97 with *R*-factors of 11.4 and 12.8%, and R_{free}-factors of 12.4 and 13.5%, respectively. The refined model coordinates have an overall rms shifts of 0.23 Å relative to the same structure determined at room temperature at 1.5 Å resolution. Several regions of the main chain and the side chains, which were not observed earlier have been seen more clearly. For example, amino acid 207, which was reported earlier as Ser has been clearly identified as Asp. Furthermore, side-chain disorders of 8 of 279 residues in the polypeptide have been identified. Hydrogen atoms appear as significant peaks in the $F_o - F_c$ difference electron density map accounting for an estimated 46% of all hydrogen atoms at 2σ level. Furthermore, the carbon, nitrogen, and oxygen atoms can be differentiated clearly in the electron density maps. Hydrogen bonds are clearly identified in the serine protease catalytic triad (Ser-His-Asp). Furthermore, electron density is observed for an unusual, short hydrogen bond between aspartic acid and histidine in the catalytic triad. The short hydrogen bond, designated "catalytic hydrogen bond", occurs as part of an elaborate hydrogen bond network, involving Asp of the catalytic triad. Though unusual, these features seem to be conserved in other serine proteases. Finally there are clear electron density peaks for the hydrogen atoms associated with the Oγ of Ser 224 and Nδ1 of His 69.

Serine proteases are present in virtually all organisms and can be intracellular or extracellular enzymes. These proteins exist as two families, the trypsin-like and the subtilisin-like families, that have been independently evolved with a similar catalytic mechanism which has been widely investigated (*1*−*5*). Both families play an important role in all the organisms through functioning in digestion, blood coagulation, post-translational processing of secreted proteins, neurotransmitters and hormones (*6*). The functional importance of catalytic triad and oxyanion hole in catalysis has been clearly established (*7*, *8*). In this mechanism, Ser functions as the primary nucleophile and His plays a dual role as proton acceptor and donor at different steps in the reaction. The role of Asp is thought to bring the His residue in the correct orientation to facilitate nucleophilic attack by Ser. Though, the overall folding of various serine proteases may differ, they all follow the same mechanism of action through an identical stereochemistry of the catalytic triad. Proteinase K (PK)[1] from *Tritirachium album* Limber (*9*) belongs to the subtilisin family as it shares a common tertiary fold with subtilisin (*10*).

To understand the functional mechanism precisely, the structures of macromolecules at atomic resolutions (1.2−0.95 Å) are required. Refinement of such structures routinely incorporates the refinement of anisotropic temperature factors which aid in the delineation of loop motion and far-ranging disorder, the recognition of hydrogen atoms, and the identification of protonation states. The disposition of hydrogen atom is critical to further our understanding of structure and function in enzymes. Native PK crystals grown under the laboratory conditions with cryocooling diffracted to about 1.3 Å with synchrotron radiation. To obtain high-quality crystals for atomic resolution data collection, crystals of PK have been grown under microgravity conditions on the space shuttle mission STS-95 using the APCF (Advanced Protein Crystallization Facility) supplied by ESA (European Space Agency) (*11*). Here, we report the results of the refinement using a complete crystallographic data set to a resolution of 0.98 Å and present a detailed structure of the PK active site. We find that the catalytic triad Asp participates in a complex hydrogen bond network that includes an unusual short hydrogen bond to His in the catalytic triad. This level of detail should now be possible to achieve for numerous enzymes due to advanced synchrotron beam line

[†] They acknowledge the financial support from the Deutsche Agentur für Luft- und Raumfahrtangelegenheiten (DLR) under Contract 50 WB 9514, the Council of Scientific and Industrial Research (CSIR), New Delhi, and the Alexander von Humboldt Foundation, Bonn.

* To whom correspondence should be addressed. Phone: +91-11-653 3931. Fax: +91-11-686 2663. E-mail: tps@aiims.aiims.ac.in.

[‡] Institute of Medical Biochemistry and Molecular Biology.

[§] Department of Biophysics.

[1] Abbreviations: PK, proteinase K; APCF, Advanced Protein Crystallisation Facility; ESA, European Space Agency.

10.1021/bi002538n CCC: $20.00
Published on Web 02/16/2001

Table 1: Crystal Data

space group	$P4_32_12$
cell dimensions (Å)	$a = b = 67.3$, $c = 106.6$
resolution range (Å)	10.0−0.98
total no. reflections observed	1 229 216
no. of unique reflections	136 380
completeness (%)	98
completeness in the highest resolution shell (1.00−0.98) (%)	95
R_{sym} (%)	3.5
R_{sym} in the highest resolution shell (1.00−0.98 Å) (%)	19.5
V_m (Å^3/Da)	2.2
solvent content (%)	45
Z	8

design that exploits short wavelength and high-intensity X-rays.

MATERIAL AND METHODS

Crystallization, Data Collection, and Data Processing. Commercially available proteinase K (E. Merck, Darmstadt) was further purified by gel filtration on a Sephadex G-75 column (150 × 2.5 cm) in 50 mM Tris-HCl, pH 7.5, containing 1 mM $CaCl_2$. Fractions of highest activity were pooled, dialyzed exhaustively at 4 °C against 1 mM calcium acetate and protein was concentrated to 30 mg/mL. To reduce the number of possible nucleation sites, the protein solution was filtered using a Microcon filtration device (Amicon) just before the loading process. For crystallization under microgravity conditions, the APCF reactors with 40 μL of protein solution reservoir were applied, mimicking the vapor diffusion method (*12*). The resulting protein/precipitant droplets were equilibrated at 22 °C with approximately 1 mL of a reservoir buffer for 8 days. After landing, the crystals were harvested in 50 mM Tris HCl, pH 6.5, 10 mM $CaCl_2$, and 1.2 M $NaNO_3$. At this time, five crystals of approximate dimensions of 0.6 × 0.5 × 0.4 mm^3 were selected for data collection, submerged for 15−60 s in a cryo-protectant solution containing 15−20% glycerol with mother liquor and subsequently shock-frozen. Crystals belonged to the tetragonal space group $P4_32_12$ with unit cell dimensions of $a = b = 67.3$ Å and $c = 106.8$ Å. The diffraction data were measured with a wavelength of 0.91 Å at DESY, Hamburg beam line X11 using a 345 mm diameter MAR-Research imaging plate detector. The data were collected in three data sets of different resolution ranges: high, medium and low, respectively. Nearly, 1.2 million reflections were observed and the merged data of 136 380 unique reflections were of 98% completeness corresponding to 0.98 Å resolution. The data collection and processing details are summarized in Table 1. It may be mentioned here that the earth grown crystals corresponding to the dimensions of 0.60 × 0.50 × 0.45 mm^3 under identical cryoconditions on the same beamline diffracted well to 1.3 Å resolution.

Refinement. Since there were significant differences between the cell parameters of the current data and those of the native structure, the initial phases were determined by molecular replacement using the program AMoRe (*13*) as implemented in the CCP4 package (*14*). The previously determined structure of PK at 1.5 Å resolution in aqueous buffer was used as the search model (*10*). Initially the structure was refined with PROLSQ (CCP4) in the 10−0.98 Å resolution range. All the temperature factors were isotropic and the refinement converged with an R-factor of 17.6% (Table 2). At this point, the hydrogen atoms for many aromatic residues and Cβ atoms were clearly seen in the difference Fourier map ($F_o - F_c$) (Figure 1a). For the protein molecule alone a total of 296 positive peaks above 3σ in the $F_o - F_c$ electron density difference Fourier map have been located at idealized hydrogen atom positions. These peaks representing approximately 16% of the 1942 hydrogen atoms expected in the protein molecule are clustered predominantly in hydrophobic and good hydrogen bond forming regions. Peaks were observed for most Cβ hydrogen atoms in 169 out of 189 residues excluding Gly and Ala residues. In addition to 3σ peaks, we observed peaks at 2σ level, which accounted for an estimated 46% of all hydrogen atoms in the protein molecule. Inclusion of hydrogen atoms gave enhanced details of other hydrogen atoms in regions of interest that had not been modeled or were detectable, falling below the 3σ threshold in previous electron density maps. These coordinates were taken for refinement using both SHELX-97 (*15*) and REFMAC for anisotropic refinement. REFMAC anisotropic refinement generates hydrogen atoms geometrically and also generates density for hydrogen atoms in separate file. At the end of the anisotropic refinement by REFMAC, the R-factor and free R-factor converged to 11.4 and 12.4%, respectively. The structure was also refined with SHELX-97. In this case, the final R and free R-factors converged to 12.8 and 13.5%, respectively (Table 2). At the end of the anisotropic refinement by both methods, the quality of electron density for the hydrogen atoms improved remarkably (Figure 1b).

Table 2: Refinement Statistics

	CCP4 PROLSQ	CCP4 REFMAC	SHELX-97
refinement	isotropic	anisotropic	anisotropic
resolutions limits (Å)	10.0−0.98		
no. of reflections	136380		
R factor (%)	17.6	11.4	12.8
free-R factor (%)	19.2	12.4	13.5
model			
protein atoms	2032		
calcium ions	2 (1 × 1, 1 × 0.5)		
water molecules	494		
nitrate atoms	32 (8 molecules)		
RMS deviations from ideal values			
bond lengths (Å)	0.007	0.008	0.013
bond angles (deg)	1.2	1.8	2.0
dihedral angles (deg)	15.6	16.4	19.2
average B factors (Å^2)			
for all atoms	12.6	12.3	2.7
water	28.5	26.8	29.1
nitrate	32.0	27.8	32.2

RESULTS AND DISCUSSION

High-Resolution Features. We have collected a 98% complete data set to 0.98 Å resolution. At this resolution, there is a dramatic increase in the quality and detail of the electron density map in comparison to the same structure determined at 1.5 Å resolution. Most notably individual heavy atoms can be differentiated. As seen from Figure 2,

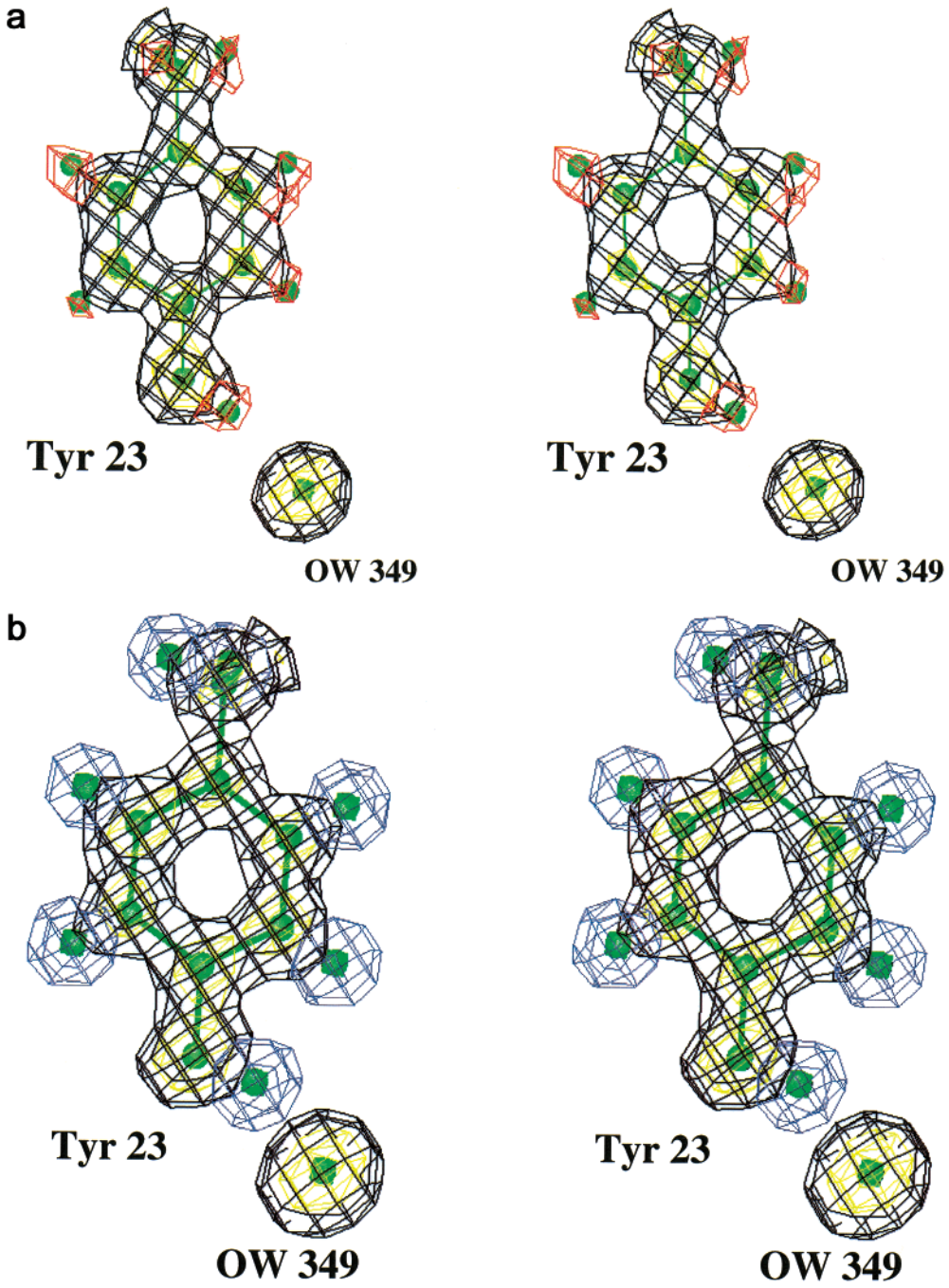

FIGURE 1: (a) ($F_o - F_c$) difference electron density map (showing a typical example of electron density for H-atoms: Tyr 23 contoured at 2.5σ (red) is superimposed on a ($2F_o - F_c$) electron density map contoured at 1σ (black) and 4σ (yellow). (b) After the refinement of H-atoms, ($2F_o - F_c$) map contoured at 1σ (black) and 4σ (yellow). The interaction of Tyr OH with a water molecule is also shown (OW 349).

the electron density in greenish color at 4σ cut off, clearly distinguishes the nitrogen atoms, from carbon atoms as the density at nitrogen atoms is larger than that of carbon atoms (*16*). There are four salt bridges found in PK structure (Figure 3, panels a−d). The residues are shown with electron density map contoured at 1σ and 4σ. In Figure 3a, the electron density for C, N, and O atoms can be distinguished based on the volume of the density contoured at 4σ. The carboxylate group in this salt bridge is expected to have a charge localized on Oδ2 of Asp 187. Oδ2 of Asp should be singly bonded to the carbon atom (Cγ) and hydrogen bonded to nitrogen atom (NH2) of Arg 12. The electron density for Oδ2 is discrete at 4σ level, while the density for the Oδ1−Cγ bond is continuous, having comparable density with carbonyl (C═O, backbone atoms) atoms of Asp 187 and Arg 12. Similar kind of density patterns are also seen for other two salt bridges. These salt bridges are shown in the Figure 3 (panels b and c). This kind of observation has also been made earlier by Kuhn et al. (*17*) in *Bacillus lentus* subtilisin. From Figure 3d, it is clearly seen that the Asp 184 is interacting through both Oδ1 and Oδ2 to two different N atoms as the charge delocalization clearly exists because the electron density is continuous on both sides of Cγ connecting Oδ1 and Oδ2 in a similar manner.

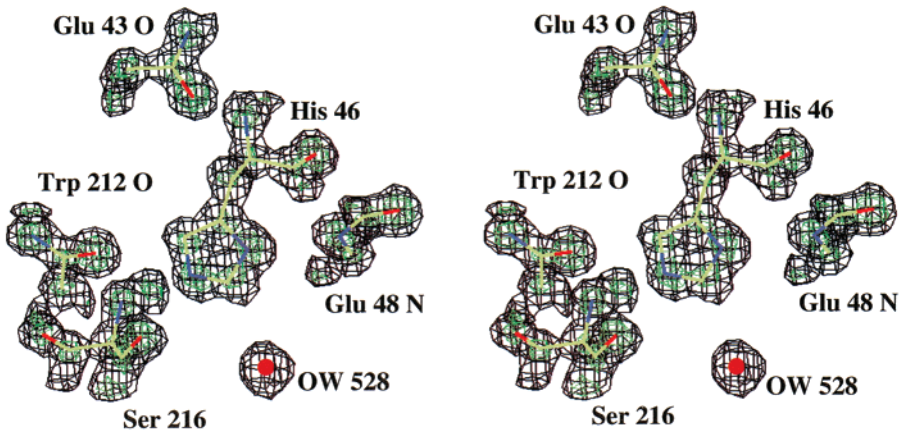

FIGURE 2: ($2F_o - F_c$) electron density map contoured at 1σ (black), 4σ (green). C, N and O atoms can be differentiated.

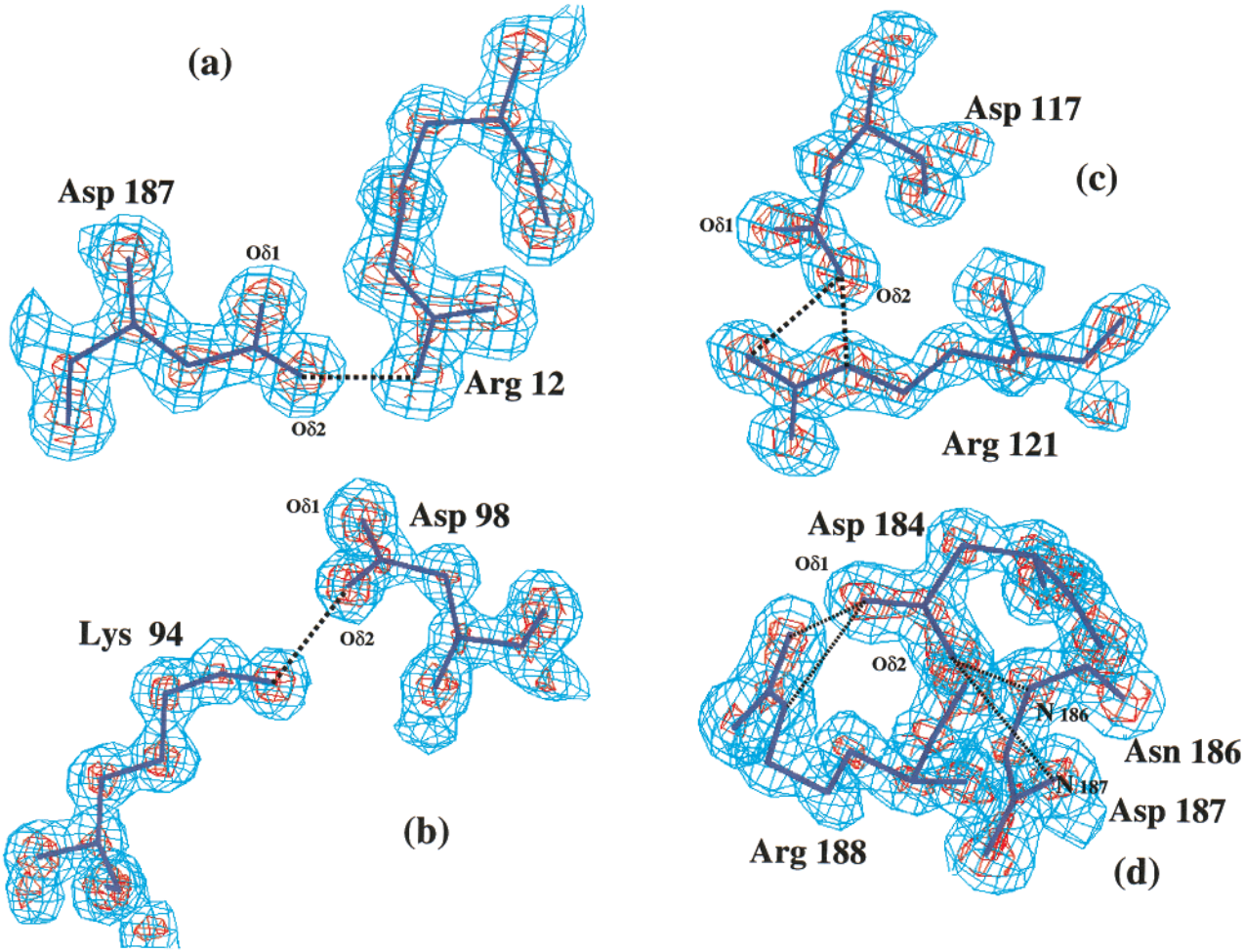

FIGURE 3: Salt bridges between (a) Asp 187−Arg 12, (b) Asp 98−Lys 94, (c) Asp 117−Arg 121, and (d) Asp 184−Arg 188. Electron density ($2F_o - F_c$) map is contoured at 1σ (blue) and 4σ (red). The presence of density toward one of the two carboxyl oxygen atoms clearly shows the presence of a double bond in the group (a−c). However, in the last bridge where both Oδ1 and Oδ2 are involved in hydrogen bonds, there is a similar density toward both oxygen atoms indicating similar partial double bond characters.

Alternate Conformations. Till now, none of the native PK structures has been reported with multiple conformations. In this structure, there are eight residues of different types (except aromatic residues), which are seen in multiple conformations. Most of these amino acids are buried inside the protein core and nearly all amino acids with alternate conformations are isolated from one another. These are shown in the Figure 4. (a) Ile 13, (b) Asp 112, (c) Asn 122, (d) Leu 131, (e) Ser 143, (f) Ser 219, (g) Ser 247, and (h) Asp 207. The 207th amino acid, which was reported earlier as Ser (*10*), but it is clearly seen here as Asp in two conformations (Figure 4h).

Solvent Structure. At the beginning of the refinement, all the 178 water molecules from the model were used for refinement. Those water molecules were retained for which the electron density in the subsequent $2F_o - F_c$ maps persisted after the refinement cycles and if they fulfilled the following criteria: within 3.4 Å of the enzyme oxygen or

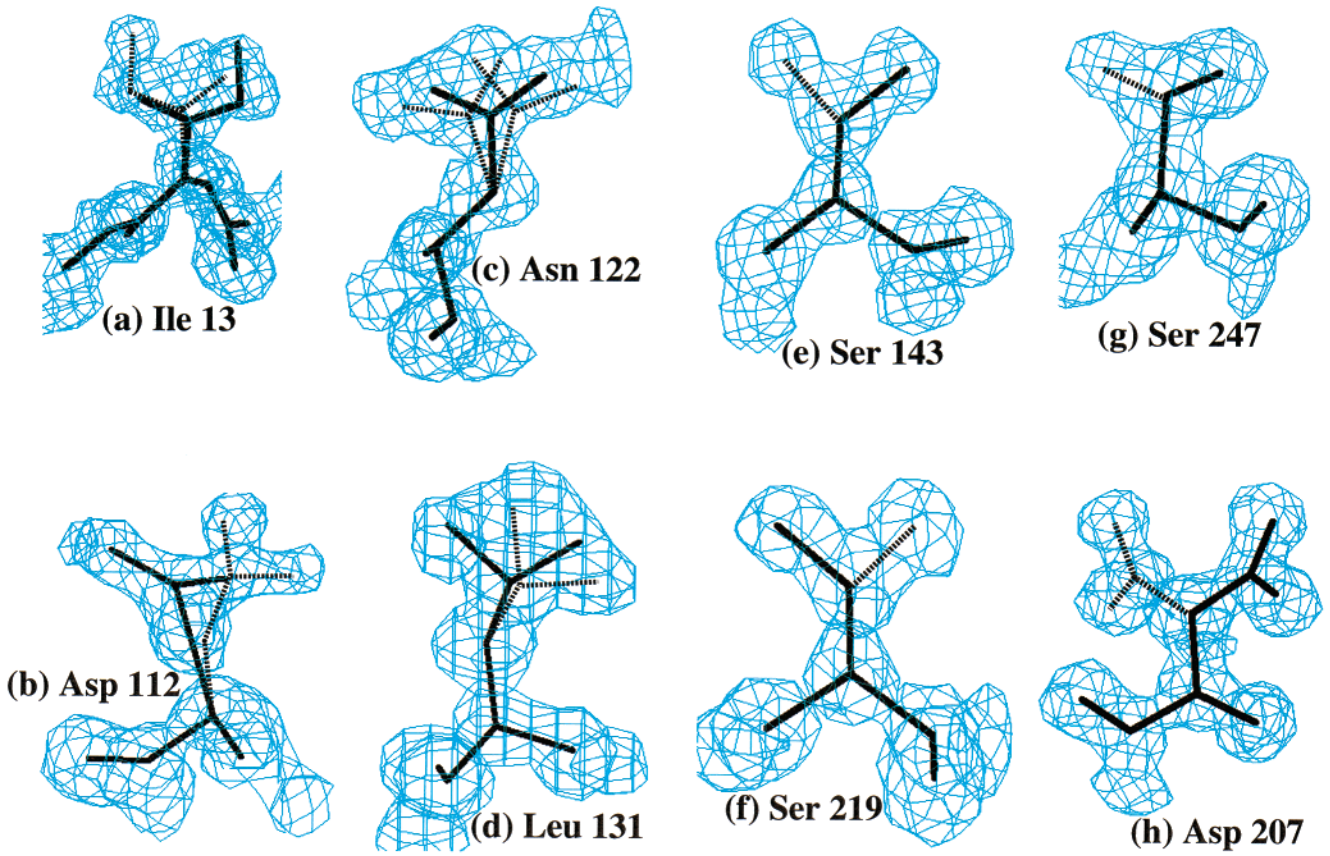

FIGURE 4: ($2F_o - F_c$) electron density map contoured at 1.2σ showing disordered residues with more than one conformations for the side chains: (a) Ile 13, (b) Asp 112, (c) Asn 122, (d) Leu 131, (e) Ser 143, (f) Ser 219, (g) Ser 247, and (h) Asp 207.

nitrogen atom, or bound to neighboring water molecule with a good hydrogen bonding geometry, *B*-factors less than 45 Å^2, and the real space correlation coefficients above 65%. Most of the original water molecules were conserved, and only around 25 water molecules on the surface were removed. Further rounds of manual building in O combined with several cycles of refinement with PROTIN/PROLSQ resulted in the inclusion of 180 additional water molecules to a total of 333 water molecules in the model. The refinement with further cycles and model building resulted in the inclusion of final 494 water molecules, in which 58 water molecules were refined with partial occupancy of 0.5 with an improvement in the final *R*-factor and free *R*-factor to 0.176 and 0.192, respectively. Final protein structure consisted of 494 water molecules with an average *B*-factor of 28.5 Å^2.

In the course of refinement, eight nitrate molecules were also identified. Nitrate molecules were distinguished from water molecules in the electron density map because at 1σ contour level, the electron densities of nitrate molecules were clearly triangular in appearance, whereas for water molecules electron densities were spherical (Figure 5a). The existence of PK-bound nitrate ions was further confirmed when we overlaid the ($2F_o - F_c$) electron density map for the enzyme in water with the refined coordinates. Most of these nitrate molecules are bound on the surface of PK. As seen from Figure 5b for example, a nitrate is bound to Arg 250 side chain in a specific manner. Two nitrate molecules were also found in the substrate binding region (Figure 5c). The average *B*-factor of the atoms of the nitrate molecules was around 30 Å^2.

C−*H*···*O Hydrogen Bonds.* The analysis of medium and high-resolution structures revealed that C−H···O bonds are ubiquitous in macromolecular structures and contribute significantly to the free energy difference between folded and unfolded states of proteins (*18*). The sum of the van der Waals radii for carbon and oxygen is 3.7 Å. The analysis of medium and high-resolution structures showed a broad minimum at 2.65 Å in the difference curve, which is shorter than 3.7 Å. Hence, these contacts can be attributed to cohesive electrostatic interactions, namely hydrogen bonds (*18*). A few high-resolution structures also reported C−H···O hydrogen bonds (*19*, *20*). A careful analysis of the present structure clearly reveals many C−H···O distances less than 3.5 Å. As an example, it is clearly seen from Figure 6 that His 46 is involved in many C−H···O type interactions. Other than Cγ, all other atoms are involved in hydrogen bonding of some kind. The electron density for this region is also shown in Figure 2.

Calcium Binding Sites. Subtilisins require calcium ions for the folding of the polypeptide chain and hence for activity (*10*, *21*). This is presumed to be a protective action by the cells against intracellular proteolysis. The intracellular calcium levels are too low to produce active enzymes, the extracellular levels are higher, and the enzyme is activated on secretion from the cell (*22*). According to the high-resolution electron density, two calcium ions were clearly identified in the structure. There are two large spherical peaks, which are involved in the coordinations with protein and water oxygen atoms. The two calcium ions Ca1 and Ca2

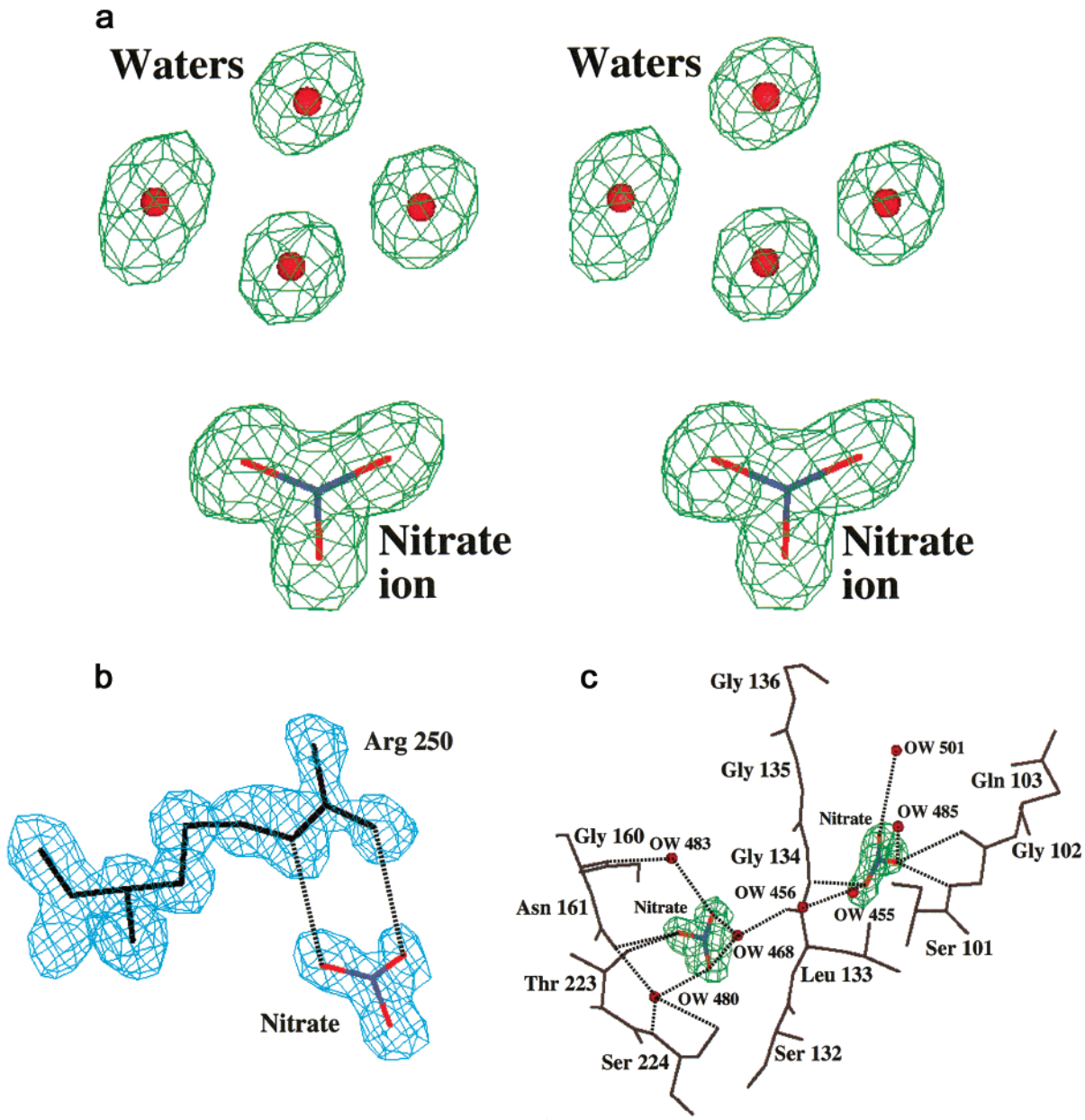

FIGURE 5: (a) Stereoview of ($F_o - F_c$) difference density map contoured at 2σ showing the difference between the shapes of densities of a nitrate ion and water molecules, (b) a nitrate ion interacting with Arg 250 on the surface of the protein molecule, (c) ($F_o - F_c$) electron density map showing the presence of two nitrate ions in the active site of the enzyme.

are located at the periphery of PK molecule and bridge loops, thereby contributing to the overall stability of the molecule. Ca1 is well defined as described earlier (*10*) and is 8-fold coordinated in the form of pentagonal bipyramid (Figure 7a).

Ca2 is less well-defined, and calcium ion in this site is partially occupied. The calcium ion bridges two loops of the amino and carboxy termini of PK. In the coordination sphere of calcium, three water molecules are also involved to complete the coordination geometry, which has a pentagonal bipyramid arrangement (Figure 7b). One of the oxygen atoms of Asp 260 and four water molecules OW 305, OW 581, OW 589, and OW 655 are in equatorial plane. The backbone oxygen atom of Thr 16 and OW 683 are at the apical positions of the pentagonal bipyramid coordination. The lower occupancy water molecules are not observed in the earlier structure (*10*). In Figure 7b, water molecules, OW 581, OW 655, and OW 683 are partially occupied.

Active Site. The catalytic triad is in the expected conformation as seen from the stereoview given in Figure 8a. The thermal ellipsoid representation of the same view is illustrated in Figure 8b. Ser 224, His 69, and Asp 39 are well ordered, and the oxygen atom (Oγ) of Ser 224 is within the hydrogen bond distance (2.99 Å) of the nitrogen atom (Nϵ2) of His 69. There is a clear peak at 3σ level in the $F_o - F_c$ electron density map between the Oγ atom of Ser 224 and Nϵ2 of His 69. The peak is situated at a distance of 1.0 Å from Oγ of Ser 224 and 2.0 Å from Nϵ2 of His 69. The hydrogen atom lies in the plane of Ser 224 and His 69 side chains and the C−H···O bond angle is 137°. This shows that the position of Oγ is in a favorable orientation to have its hydrogen atom abstracted by His 69. The distance between the nitrogen atom (Nδ1) of His 69 and the oxygen atom (Oδ2) of Asp 39 is 2.68 Å. Furthermore, a 3σ peak in the $F_o - F_c$ electron density map is found between these atoms (Figure 8a). The

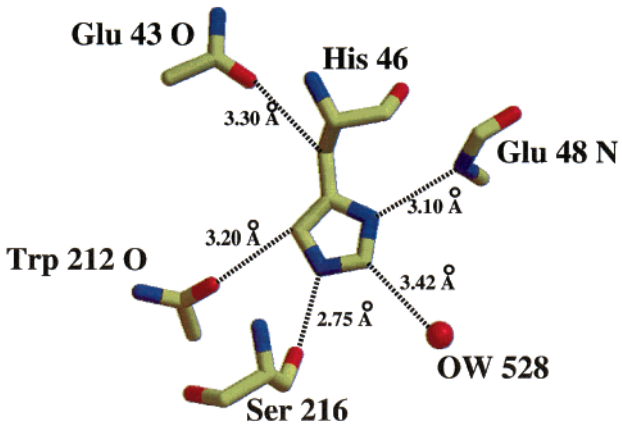

FIGURE 6: Example of C−H···O hydrogen bonds involving His 46 in the structure.

peak is situated at a distance of 1.0 Å from Nδ1 of His 69 and 1.6 Å from Oδ2 of Asp 39. The hydrogen atom participating in this short hydrogen bond within the catalytic triad is in the plane of His 69 and Asp 39 side chains and is only slightly skewed toward Oδ1 of Asp 39. The Nδ1−H···Oδ2 bond angle is 169°. The short bond distance between Asp 39 and His 69 is the same in the 1.5 Å room-temperature structure of native PK (*10*) and various other structures of PK with and without inhibitors bound (*23*−*29*). Therefore, the occurrence of the short hydrogen bond is not an artifact of cryocooling. Similar observations have also been made in several structures of trypsin (*30*) as well as in the structure of homodimeric serine carboxypeptidase II from wheat (*31*), subtilisin BPN′ (*32*) and *Bacillus lentus* subtilisin (*17*). The corresponding distance is also short in these structures though the interactions between the catalytic Asp and neighboring residues differ considerably. For example, in the present structure, Asp 39 Oδ2 forms two additional hydrogen bonds with proton donors Thr 40 N (2.71 Å) and Gly 70 N (3.10 Å) while Asp 39 Oδ1 makes an additional hydrogen bond to solvent water OW 328 (2.67 Å). In trypsin Asp 102 Oδ2 makes a second hydrogen bond to Ser 214 while Asp 102 Oδ1 is within a hydrogen bond distance of Ala 56. In serine carboxypeptidase II, Asp 338 Oδ2 is involved in two additional hydrogen bonds to proton donors, Asn 176 and Val 342.

On the other hand, some of the structures of related enzymes available at high resolutions do not report short hydrogen bonds between His and Asp of the catalytic triad. A compilation with several examples of normal hydrogen bond distances is available (*5*). The thermal motions of the side chains of three residues of the catalytic triad are identical. The electron densities for the hydrogen atoms of Ser 224 Oγ and His 69 Nδ1 have been clearly observed in this structure (Figure 8a). This has not yet been observed in any other high-resolution structure reported so far, including the ultra-high-resolution (0.78 Å) structure of *Bacillus lentus* subtilisin (*17*), presumably due to a degree of mobility of the respective atoms in the structure. The electron density of the carboxylic group in Asp 39 indicates that Oδ2 is only partially charged and not negatively charged as suggested by some previous investigations (*5*, *33*, *34*). The atomic resolution structure of PK provides a clear picture of the locations of protons in the catalytic triad and reveals the nature of interactions between Asp−His and His−Ser. Therefore, the availability of high-resolution data has provided a much more detailed picture of the serine protease catalytic triad. While general features are conserved, the detailed interaction for the catalytic aspartic acid residue vary in different classes of serine proteases. We are able to confirm the existence of a special hydrogen bond as observed earlier in subtilisin (*17*). Furthermore, we have been able to

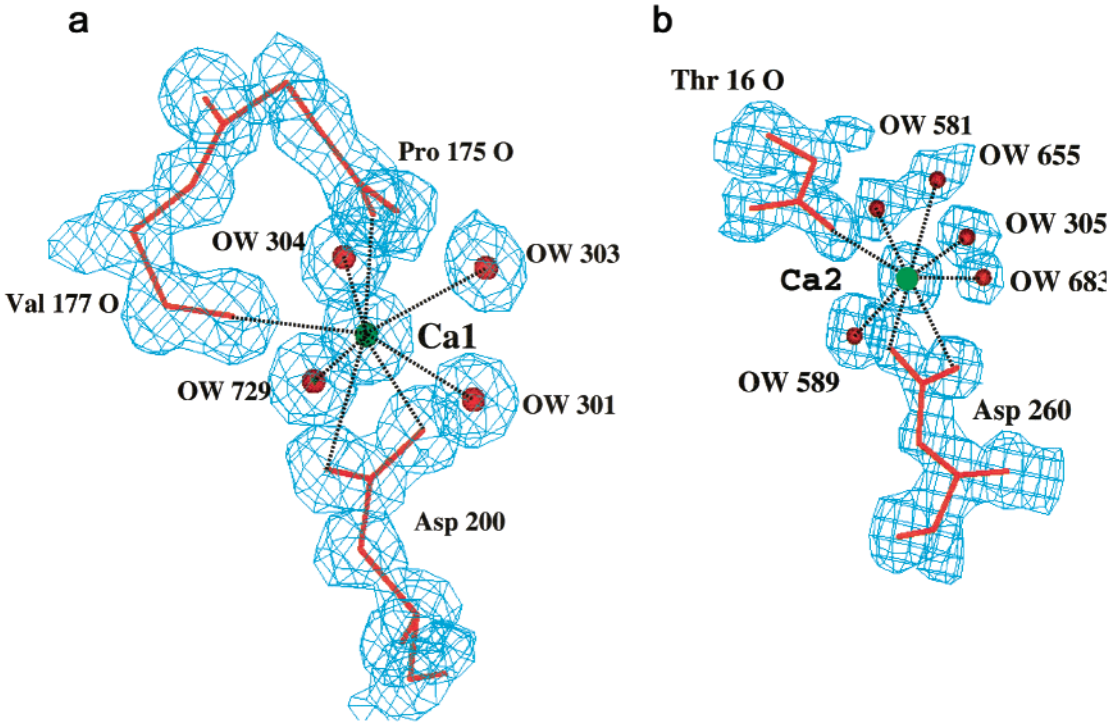

FIGURE 7: (a) ($2F_o - F_c$) electron density map contoured at 1σ showing the coordination geometry of **Cal**, (b) ($2F_o - F_c$) electron density map contoured at 1σ showing the coordination geometry of **Ca2** in the structure.

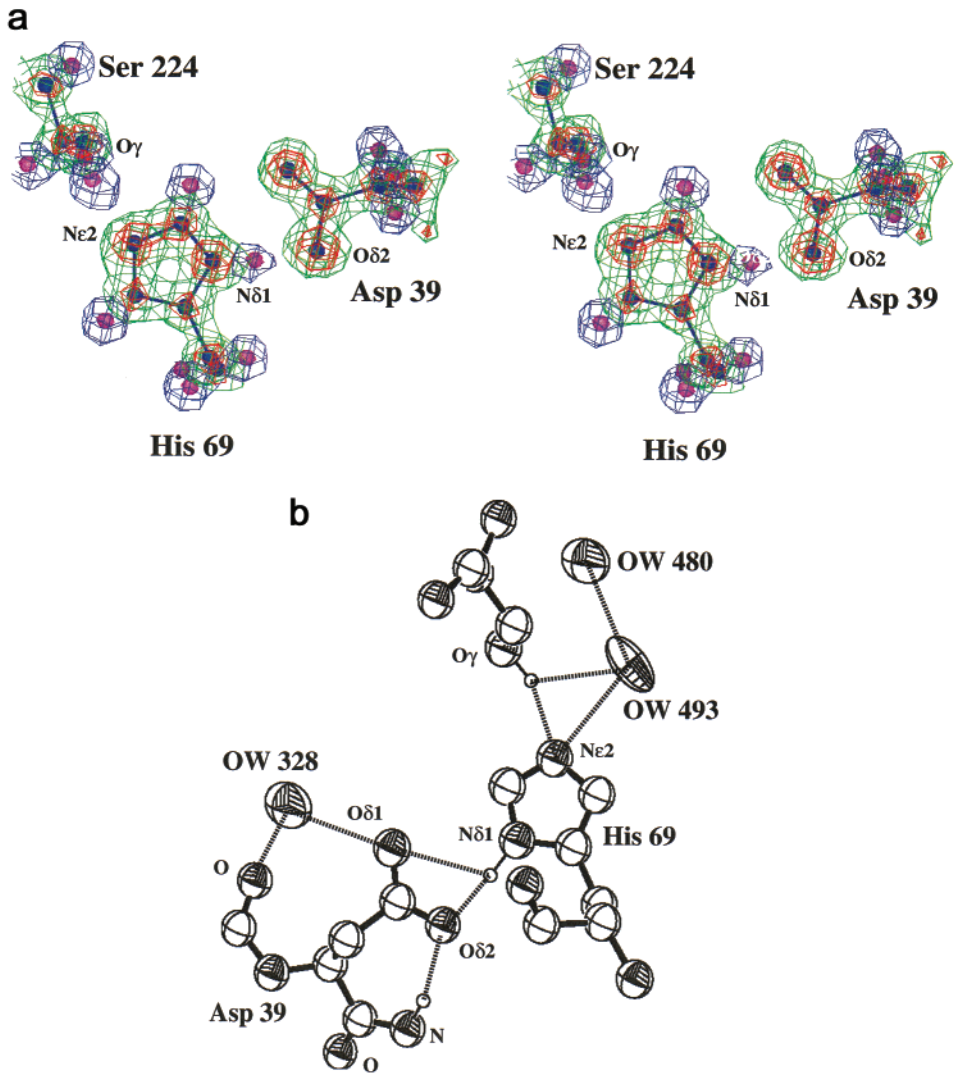

FIGURE 8: Catalytic triad. (a) Stereoview displaying model H superimposed on the ($F_o - F_c$) map (model H phases) at 1σ (green) and 4σ (red). The hydrogen atom densities (blue: 2σ in difference map) are clearly seen between Ser 224 Oγ and His 69 Nϵ2, and His 69 Nδ1 and Asp 39 Oδ2, (b) schematic representation of the catalytic residues and hydrogen bonded neighbors with thermal ellipsoid representation centered at 50% probability.

observe the positions of hydrogen atoms in the catalytic triad. These will provide a solid structural basis for understanding of the mechanism of action of serine proteases.

ACKNOWLEDGMENT

The authors thank ESA and NASA for the opportunity to crystallize samples under microgravity.

REFERENCES

1. Blow, D. M. (1976) *Acc. Chem. Res. 9*, 145−142.
2. Tsukuda, H., and Blow, D. (1985) *J. Mol. Biol. 184*, 703−711.
3. Bone, R., Shenvi, A. B., Kettner, C., and Agard, D. A. (1987) *Biochemistry 26*, 7609−7614.
4. Siezen, R. J., Willem, M. V., Leunissen, J. A. M., and Dikstra, B. W. (1991) *Protein Eng. 4*, 719−737.
5. Lange, G., Betzel, Ch., Branner, S., and Wilson, K. S. (1994) *Eur. J. Biochem. 224*, 507−518.
6. Neurath, H. (1986) *J. Cell. Biochem. 32*, 35−49.
7. Russel, A. J., and Fersht A. R. (1987) *Nature 328*, 496−500.
8. Carter, P., and Wells, J. A. (1988) *Nature 332*, 564−568.
9. Ebeling, W., Hennrich, N., Klockow, M., Metz, H., Orth, H. U., and Lang, H. (1974) *Eur. J. Biochem. 47*, 91−97.
10. Betzel, Ch., Pal, G. P., and Saenger, W. (1988) *Eur. J. Biochem. 178*, 155−171.
11. Bosch, R., Lautenschlager, P., Potthast, L., and Stapelmann, J. (1992) *J. Crys. Growth 122*, 310−314.
12. McPherson, A. (1985) *Methods Enzymol 114*, 112−120.
13. Navaza, J. (1994) *Acta Crystallogr., Sect. A 50*, 157−163.
14. Collaborative Computational Project, Number 4. (1994) *Acta Crystallogr., Sect. D 50*, 760−767.
15. Sheldrick, G., and Schneider, T. (1997) *Methods Enzymol. 277*, 319−343.
16. Deacon, A., Gleichmann, T., Kalb (Gibsoa), A. J., Price, H., Raftery, J., Bradbrook, G., Yariv, J., and Helliwell, J. R. (1997) *J. Chem. Soc., Faraday Trans. 93*, 4305−4312.
17. Kuhn, P., Knapp, M., Soltis, S. M., Ganshaw, G., Thoene, M., and Bott, R. (1998) *Biochemistry 37*, 13446−12452.
18. Derewenda, Z. S., Lee, L., and Derewenda, U. (1995) *J. Mol. Biol. 252*, 248−262.
19. Lubkowski, J., Dauter, Z., Yang, F., Alexandratos, J., Merkel, G., Skalka, A. M., and Wlodawer. A. (1999) *Biochemistry 38*, 13512−13522.
20. Ridder, I. S., Rozeboom, H. J., and Dijkstra, B. W. (1999) *Acta Crystallogr., Sect. D 55*, 1273−1290.
21. Betzel, Ch., Teplyakov, A. V., Harutyunyan E. H., Saenger, W., and Wilson K. S. (1990) *Protein Eng. 3*, 161−172.
22. Voordouw, G., Milo, C., and Roche, R. S. (1976) *Biochemistry 15*, 3716−3724.

23. Betzel, C., Pal, G. P., Struck, M., Jany, K. D., and Saenger, W. (1986) *FEBS Lett 197*, 105−110.
24. Betzel, C., Bellemann, M., Pal, G. P., Bajorath, J., Saenger, W., and Wilson K. S. (1988) *Proteins: Struct., Funct., Genet. 4*, 157−164.
25. Betzel, C., Singh, T. P., Visanji, M, Peters, K., Fittkau, S., Saenger, W., and Wilson, K. S. (1993) *J. Biol. Chem. 268*, 15854−15858.
26. Wolf, W. M., Bajorath, L., Muller, A., Raghunathan, S., Singh, T. P., Hinrichs, W., and Saenger, W. (1991) *J. Biol. Chem. 266*, 17695−17699.
27. Saxena, A. K., Singh, T. P., Peters, K., Fittkau, S., Wilson, K. S., and Betzel, C. (1996) *Proteins: Struct., Funct., Genet. 25*, 195−201.
28. Saxena, A. K., Singh, T. P., Peters, K., Fittkau, S., and Betzel, C. (1996) *Protein Sci. 5*, 2453−2458.
29. Gupta, M. N., Tyagi, R., Sharma, S., Karthikeyan, S., and Singh, T. P. (2000) *Proteins: Struct., Funct., Genet. 239*, 226−234.
30. Marquart, M., Walter, J., Deisenhofer, J., Bode, W., and Huber, R. (1983) *Acta Crystallogr., Sect. B 29*, 480−490.
31. Liao, D. I., Breddam, K., Sweet, R. M., Bullock, T., and Remington, S. J. (1992) *Biochemistry 31*, 9796−4812.
32. Bott, R., Ultsch, M., Kossiakoff, A., Graycar, T., Katz, B., and Power, S. (1988) *J. Biol. Chem. 263*, 7895−7906.
33. Longhi, S., Czejek, M., Lamzin, V., Nicolas, A., and Cambillau, C. (1997) *J. Mol. Biol. 268*, 779−799.
34. Frey, P. A., Whitt, S. A., and Tobin, J. B. (1994) *Science 264*, 1927−1930.

BI002538N